Received: 23 September 2023 | Revised: 16 January 2024 | Accepted: 16 March 2024

DOI: 10.33012/navi.643

ORIGINAL ARTICLE

Real-Time Precise Point Positioning Method Considering Broadcast Ephemeris Discontinuities

Quanrun Cheng[1,2] | **Junping Chen**[1,2] | **Yize Zhang**[1,2] | **Chao Yu**[1,2]

[1] Shanghai Astronomical Observatory, Chinese Academy of Sciences, Shanghai 200030, China

[2] School of Astronomy and Space Science, University of Chinese Academy of Sciences, Beijing 100049, China.

Correspondence
Junping Chen
Shanghai Astronomical Observatory, Chinese Academy of Sciences, Shanghai 200030, China,
Email: junping@shao.ac.cn.

Abstract

With advancements in the broadcast ephemeris accuracy of global navigation satellite systems (GNSSs), precise point positioning based on broadcast ephemeris (BE-PPP) is gradually showing promising prospects. However, the periodic updates of GNSS ephemeris result in discontinuities in the satellite orbit and clock offset during handovers. These discontinuities can significantly impact positioning accuracy. In this study, we calculate the combined ephemeris discontinuities, which indicate a linear combination of satellite radial orbit and clock discontinuities. We then compensate for the combined ephemeris discontinuities in the subsequent satellite clocks prior to positioning. For BeiDou Navigation Satellite System 3 (BDS-3) and the Global Positioning System (GPS), the three-dimensional (3D) position accuracy in kinematic mode is improved by 30–50 cm, reaching 33.9 cm. For GPS/Galileo/BDS-3 triple-constellation kinematic solutions, the accuracy reaches 23.2 cm. In static mode, the 3D position accuracy is 14.6 cm for BDS-3-only positioning and 15.1 cm for GPS. For GPS/Galileo/BDS-3 triple-constellation static BE-PPP solutions, the 3D position accuracy improves to 8 cm.

Keywords

broadcast ephemeris discontinuity, precise point positioning, signal-in-space range error

1 | INTRODUCTION

Precise point positioning (PPP) has been developed for over 30 years since it was first put forward in 1990 (Malys & Jensen, 1990; Zumberge et al., 1997). The original PPP approach used post-processed precise products provided by the International Global Navigation Satellite System (GNSS) Service (IGS), and later, real-time products delivered over the network were also developed (J. Chen et al., 2013; Hadas & Bosy, 2015; Elsobeiey & Al-Harbi, 2016). The positioning accuracy of real-time PPP based on the BeiDou Navigation Satellite System (BDS) real-time product is 14 cm in kinematic mode and 4 cm in static mode (Pan et al., 2020). Recently, real-time products have been broadcasted via satellites, such as the orbit and clock corrections broadcast by the B2b signal of BDS, enabling users in the Asia-Pacific region to obtain decimeter-level kinematic positioning and centimeter-level static positioning results (Yang et al., 2019, 2022; CSNO, 2020; Chen, Zhang et al., 2022).

However, the availability of satellite-based real-time corrections is currently limited to geostationary orbit (GEO) satellites, which restricts their application in other parts of the world. To overcome this limitation, researchers have extensively studied PPP based on broadcast ephemeris (BE-PPP). It has been shown that BE-PPP with Galileo and the Global Positioning System (GPS) can provide a positioning accuracy of a few decimeters when post-processed products or real-time orbit and clock streams are not available (Carlin et al., 2021; Hadas et al., 2019). With the improved accuracy of the BDS-3 orbit and clock offset (Geng et al., 2022), BE-PPP for BDS has become feasible and offers better accuracy than standard point positioning (G. Chen et al., 2022), but lower accuracy than traditional PPP (Hadas et al., 2019).

Carlin et al. (2021) conducted GPS/Galileo-integrated BE-PPP and estimated the signal-in-space range error (SISRE), which represents the projected orbit and clock errors introduced by the broadcast ephemeris, and obtained a significant improvement in positioning accuracy. Time transfer experiments using a similar method achieved an accuracy of 0.5 ns (Carlin et al., 2022). The researchers reported that the discontinuity of the orbit and clock offset is caused by the handover of broadcast ephemeris and developed a model to account for variations in these errors using the SISRE process noise. This model proved effective for GPS and Galileo systems. Following Carlin's strategy, G. Chen et al. (2022) conducted BE-PPP for BDS-3/Galileo/GPS and integrated the three systems. The authors also considered systematic rotation errors of BDS-3 orbits. To mitigate the impact of large discontinuities, they used the magnitude of the ephemeris discontinuity to determine whether to reset the initial variance of the SISRE. However, time was still required to reconverge and accurately reflect the SISRE when the ephemeris was updating, regardless of whether the reset was performed. The ephemeris discontinuity is composed of both an orbit and clock offset discontinuity. Compared with the orbit discontinuity, the clock offset discontinuity has been shown to have a greater contribution to the ephemeris discontinuity (G. Chen et al., 2022). Consequently, it is necessary to develop approaches for mitigating the impact of the ephemeris discontinuity.

To address this issue, this paper proposes a method to ensure a continuous ephemeris by considering broadcast ephemeris jumps during handovers. First, a modified broadcast clock offset (MBCO) is introduced, which can suppress the impact of ephemeris discontinuities. Subsequently, the static and kinematic PPP performance is evaluated by using the MBCO. Finally, concluding remarks are given.

2 | BDS-3/GPS BROADCAST EPHEMERIS DISCONTINUITY AND ITS IMPACT ON POSITIONING

To gain a better understanding of the impact of discontinuity on GPS and BDS-3 positioning, we conducted a BE-PPP analysis on June 1, 2021, in kinematic mode at the CHPG, BILL, and GAMG stations. We excluded the results for Galileo, as the discontinuity had a minimal effect on its positioning. The stations used in this study, information regarding observations, and PPP processing configurations are presented in Table 1, Table 2, and Table 3.

In general, the ephemeris update interval is 2 h for GPS, 1 h for BDS-3, and 10 min for Galileo. The clock discontinuity for BDS-3 is the most significant, resulting in an average distance conversion of approximately 0.3 m, sometimes exceeding 1 m. In contrast, GPS exhibits a smaller discontinuity, typically within 0.2 m,

TABLE 1
Settings for the Positioning Strategy
"BRD" and "mBRD" refer to "using the original broadcast ephemeris" and "using the MBCO," respectively. "sto" and "est" indicate "considered only in the stochastic model" and "estimated SISRE." "(GC,G)" denotes the use of GPS and BDS-3 satellites, with the MBCO applied only for GPS. "(GCE,GC)" indicates the use of GPS, BDS-3, and Galileo satellites, with the MBCO applied for GPS and BDS-3. Similar rules were applied to the remaining configurations. n/a: not applicable.

	Estimate SISRE	Initial variance (σ_0) & process noise (σ_P)	Stochastic model	σ_{eph}	Ephemeris used
BRD_sto(C)	No	n/a	Yes	15 cm	BDS-3 raw broadcast
BRD_est(C)	Yes	30 cm & 7 cm	No	0	BDS-3 raw broadcast
mBRD_sto(C)	No	n/a	Yes	9 cm	BDS-3 modified broadcast
mBRD_est(C)	Yes	20 cm & 4 cm	No	0	BDS-3 modified broadcast
BRD_sto(G)	No	n/a	Yes	20 cm	GPS raw broadcast
BRD_est(G)	Yes	35 cm & 8 cm	No	0	GPS raw broadcast
mBRD_sto(G)	No	n/a	Yes	10 cm	GPS modified broadcast
mBRD_est(G)	Yes	30 cm & 6 cm	No	0	GPS modified broadcast
mBRD_est(GC,C)	Yes	BDS-3: 20 cm & 4 cm GPS: 35 cm & 8 cm	No	0	BDS-3 modified broadcast with GPS raw broadcast
mBRD_est(GC,G)	Yes	BDS-3: 30 cm & 7 cm GPS: 30 cm & 6 cm	No	0	GPS modified broadcast with BDS-3 raw broadcast
mBRD_est(GCE,G)	Yes	BDS-3: 30 cm & 7 cm GPS: 30 cm & 6 cm Galileo: 12 cm & 3 cm	No	0	GPS modified broadcast with BDS-3 and Galileo raw broadcast
mBRD_est(GCE,C)	Yes	BDS-3: 20 cm & 4 cm GPS: 35 cm & 8 cm Galileo: 12 cm & 3 cm	No	0	BDS-3 modified broadcast with GPS and Galileo raw broadcast
mBRD_est(GCE,GC)	Yes	BDS-3: 20 cm & 4 cm GPS: 30 cm & 6 cm Galileo: 12 cm & 3 cm	No	0	GPS and BDS-3 modified broadcast with Galileo raw broadcast

TABLE 2
Details of the IGS Stations

Name	Receiver	Antenna	Latitude	Longitude
BILL	SEPT POLARX5	TRM59800.99	33.578	−117.065
CHPG	TRIMBLE ALLOY	TRM59800.00	−22.682	−45.002
DJIG	SEPT POLARX5	TRM59800.00	11.526	42.847
GAMG	SEPT POLARX5TR	LEIAR25.R4	35.590	127.920
HOFN	LEICA GR50	LEIAR25.R4	64.267	−15.198
KRGG	TRIMBLE ALLOY	LEIAR25.R4	−49.352	70.256
LMMF	TRIMBLE ALLOY	TRM57971.00	14.595	−60.996
MCHL	TRIMBLE ALLOY	TRM59800.00	−26.359	148.145
MKEA	SEPT POLARX5	JAVRINGANT_DM	19.801	−155.456
OHI3	EICA GR50	LEIAR25.R4	−63.321	−57.901
URUM	JAVAD TRE_3	JAVRINGANT_G5T	43.808	87.601

whereas Galileo experiences an extremely low discontinuity, usually less than 5 cm (Carlin et al., 2022; G. Chen et al., 2022).

Figure 1 illustrates the impact of the broadcast ephemeris discontinuity on BDS-3. All three stations in the study were affected, experiencing sudden orbit and clock changes that introduced errors into the coordinate parameters. The most

TABLE 3
Process Configuration

Item	Description
GNSS observations	Ionospheric-free combination of GNSS carrier phase and pseudorange, 30-s sampling
Frequencies	B1C & B2a for BDS-3 L1 & L2 for GPS E1 & E5a for Galileo
Elevation cut-off angle	10°
Observable weighting	Comprehensive consideration of satellite system, elevation angle
Orbit and clock	Original broadcast ephemeris for BRD_sto and BRD_est; MBCO for BRD_est and mBRD_est
Processing sessions	Daily solutions of 24 h
Relativistic effect	Corrected
Solid earth tide	Corrected
Ocean tide	Corrected
Receiver clock offset	Estimated as white noise
Tropospheric dry delay	Saastamoinen model and Vienna mapping function 1
Tropospheric wet delay	Estimated as a random walk ($2\text{cm}/\sqrt{\text{h}}$) with Vienna mapping function 1
SISRE	Estimated as a random walk in BRD_est and mBRD_est; ignored in BRD_sto and mBRD_sto
Ambiguity	Estimated as a constant for each ambiguity arc

significant impact is observed in the up component, with errors exceeding 1 m at specific times, such as 5 h, 11 h, and 12 h for CHPG, 5 h, 13 h, and 20 h for BILL, and 1 h, 4 h, 9 h, and 16 h for GAMG. Although the impact on the east and north components is relatively small, discontinuity errors are still present at the decimeter level.

Research conducted by G. Chen et al. (2022) revealed significant discontinuities in the BDS-3 ephemeris. Figure 2 and Figure 3 present the average 24-h absolute error time series of 11 stations over a period of 7 days. For BDS-3, the shifts are obvious, occurring when the broadcast ephemeris updates. For the north and east components, the jumps are relatively small, generally within 5 cm. In contrast, for the up component, the jumps are greater than 10 cm. These results confirm the strong correlation between the deterioration in positioning accuracy and the broadcast ephemeris switch.

For GPS, the correlation is less frequent but still observable, as shown in Figure 3. Differing from BDS-3, we did not switch to the new broadcast ephemeris as soon as it became available. Instead, we used the broadcast ephemeris closest to the positioning moment for the calculation. Thus, the ephemeris switch in the positioning program occurs at the midpoint between the two sets of ephemerides, corresponding to odd-numbered hours. For example, at 3 h, 9 h, 11 h, 19 h, and 23 h, there are obvious discontinuities in the positioning time series, particularly noticeable in the up component. These obvious discontinuities generally reach approximately 0.1 m, significantly impacting the positioning accuracy.

By comparing the positioning error time series of BDS-3 with that of GPS, we conclude that the obvious discontinuities in the positioning error time series result from ephemeris switching. BDS-3 experiences these discontinuities more

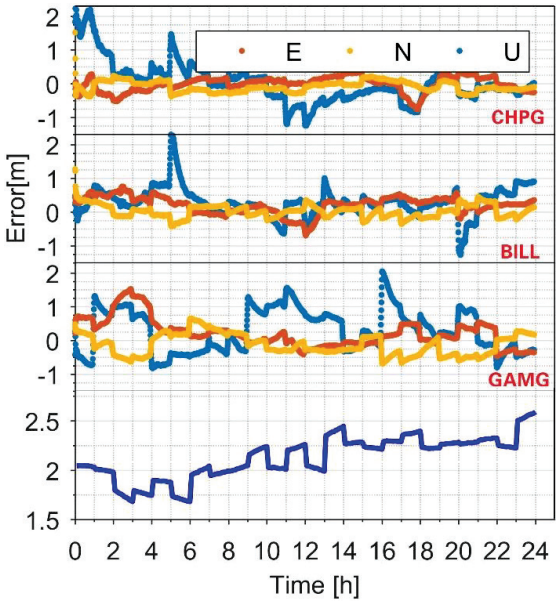

FIGURE 1 Time series of BE-PPP errors for BDS-3 in kinematic mode at stations CHPG, BILL, and GAMG
From top to bottom, the lines represent the time series of positioning errors for three stations and the time series of the average absolute values of clock offsets for all BDS-3 satellites.

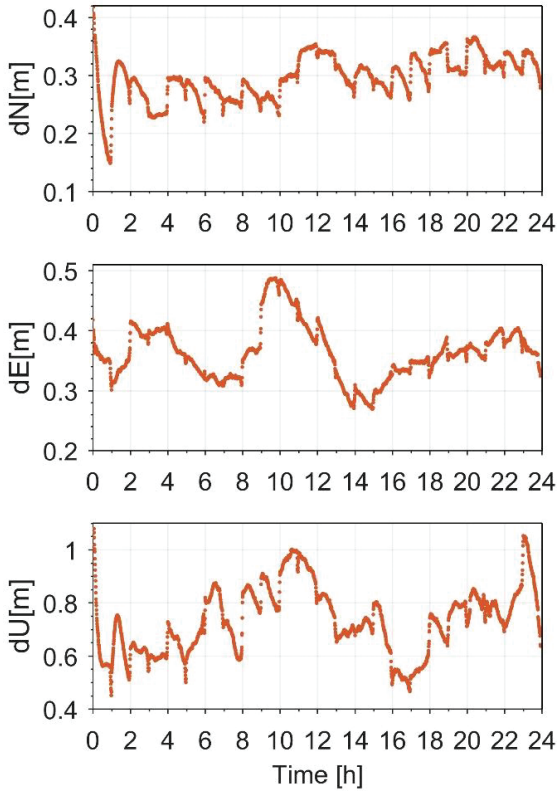

FIGURE 2 Average time series of the absolute error in BE-PPP for BDS-3 observed at 11 stations from June 1 to 7, 2021

frequently and with greater magnitude, whereas for GPS, the discontinuities occur less frequently and are on a smaller scale. These findings highlight the need for an improved approach to handle discontinuities in BDS-3 and GPS systems.

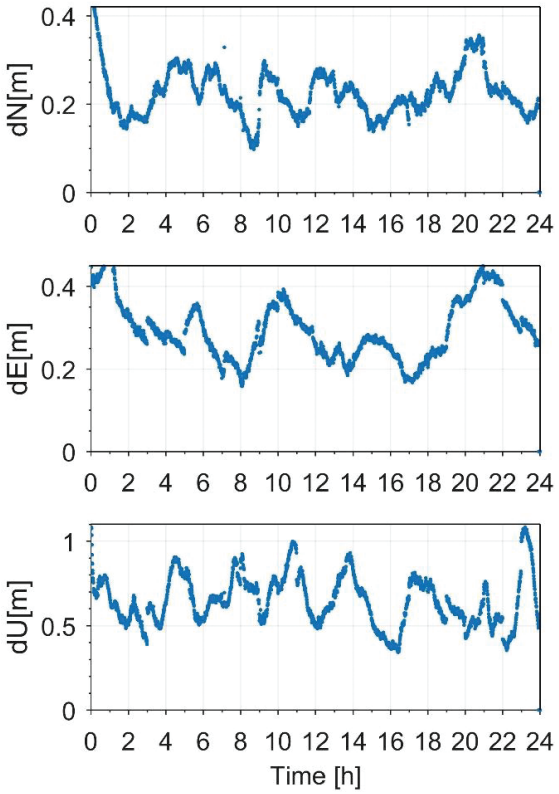

FIGURE 3 Average time series of the absolute error in BE-PPP for GPS observed at 11 stations from June 1 to 7, 2021

3 | CONCEPT AND ACCURACY EVALUATION OF THE MBCO

The error in the ephemeris consists of two parts: orbit error and clock error. Correspondingly, the discontinuities in the ephemeris also consist of orbit and clock discontinuities. Considering the definition of SISRE given by Montenbruck et al. (2015) and G. Chen et al. (2022), the discontinuity in the ephemeris is defined as follows:

$$dSIS = \sqrt{(\alpha \cdot dR - c \cdot d\tau)^2 + \beta^2 \left(dA^2 + dC^2\right)} \tag{1}$$

where dA, dC, and dR are the along-track, cross-track, and radial component of orbit discontinuity, respectively. $d\tau$ denotes the clock discontinuity. c denotes the speed of light in vacuum, and α and β denote the contribution of the orbit discontinuity to $dSIS$.

Equation (1) is a scalar representing the absolute value of overall differences between two subsequent ephemerides. Considering that the ephemeris discontinuity is directional and the contributions to the discontinuity of the along- and cross-track components are relatively small, we refer to the definition of Zhang et al. (2020) and define the ephemeris discontinuity as follows:

$$dSIS = \alpha \cdot dR - c \cdot d\tau \tag{2}$$

In the definition of $dSIS$ from Equation (2), the parameters related to the along- and cross-track direction of the orbit are omitted, and $dSIS$ transforms from a

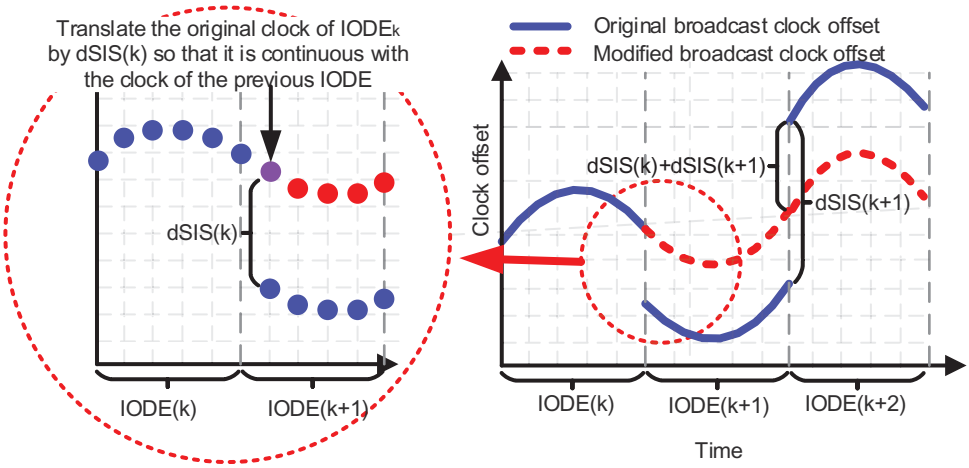

FIGURE 4 Diagram of the MBCO
The right side shows the variation in clock offset, and the left side shows the discontinuity in detail.

scalar to a vector. In Equation (2), α has a value of 0.982, 0.992, and 0.980 for BDS-3 medium earth orbit, BDS inclined geosynchronous orbit/GEO, and GPS satellites (Chen, Wang et al., 2022).

We assume that the initial user positioning requirement is in the k-th issue of data ephemeris (IODE), which is represented as $IODE(k)$. The user receives the navigation message from the satellites and calculates the orbit and clock based on the current $IODE$. This set of orbit and clock values is then extrapolated and used continuously until a new navigation message becomes available. However, if the new navigation message is used directly for positioning, reconvergence issues can arise. To avoid this problem, an additional step is performed before the new navigation messages are incorporated into the positioning solution.

First, the $dSIS(k)$ between the new and old ephemeris in the same epoch is calculated after the new navigation message, which is shown in the red circle on the left side of Figure 4, is received. The $dSIS(k)$ must be converted into a time quantity by dividing by the speed of light. The solid blue circle represents the clock offset calculated from the original broadcast ephemeris, showing a discontinuity between the two $IODEs$. By compensating $dSIS(k)$ in the clock $CLK(k+1)$ of $IODE(k+1)$, the clock values between the two $IODEs$ can be linked together, effectively eliminating the discontinuity introduced by the ephemeris. If the positioning calculation extends across multiple $IODEs$, an accumulation operation for $dSIS(k)$ is necessary to ensure a smooth transition. Figure 5 provides an overview of the overall MBCO process.

Figure 6 illustrates the time series of clock errors for 12 satellites, along with their daily averages, for June 1, 2021. The top four satellites correspond to BDS-3, the middle four represent GPS, and the bottom four represent Galileo. The precise product from the German Research Center for Geosciences serves as a reference, and the time group delay correction is applied. In Figure 6, it can be observed that all satellite clocks exhibit a satellite-specific timescale bias when compared with the precise products (Montenbruck et al., 2015). However, in positioning applications, this bias can be largely compensated for by the ambiguity parameter. Notably, the original BDS-3 broadcast ephemeris displays noticeable discontinuities at whole hours, occasionally resulting in differences of up to 1 m. The errors induced by ephemeris discontinuities will affect the positioning results during ephemeris updates and will gradually be absorbed by the ambiguity parameters. However,

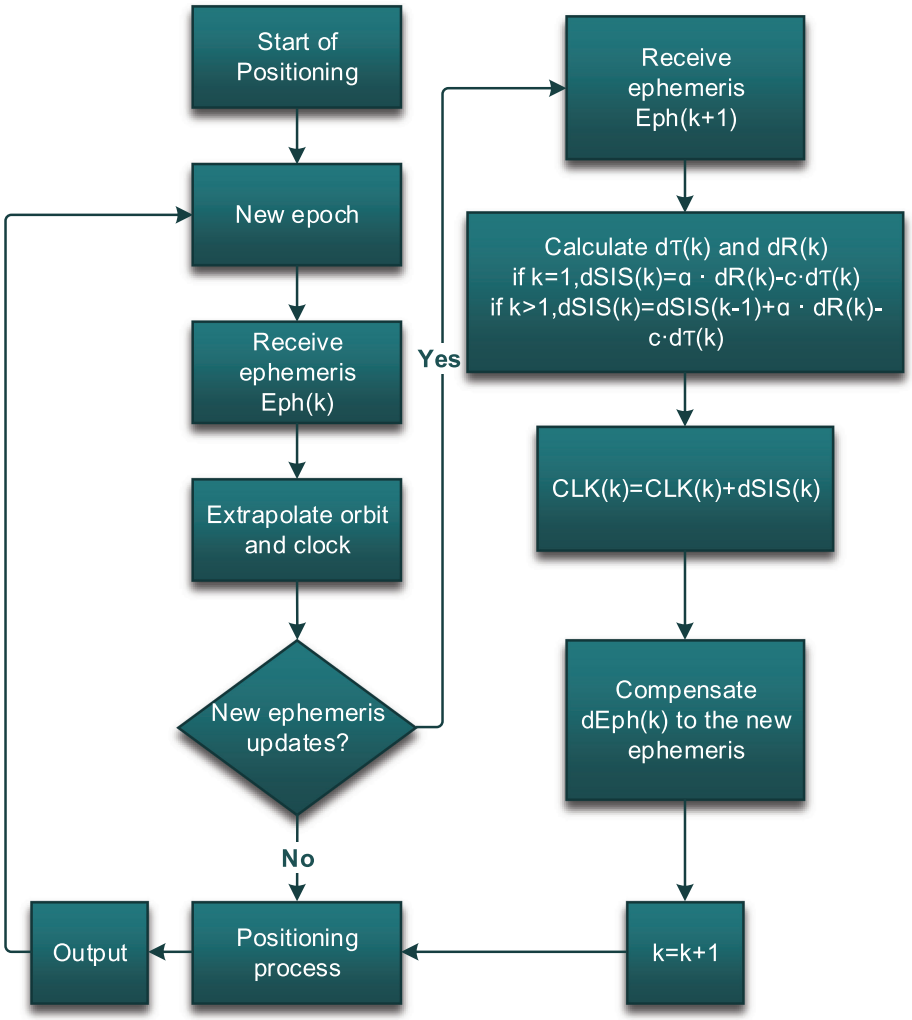

FIGURE 5 Flow chart for generating the MBCO

this process takes time and results in a significant period of reconvergence. The use of the MBCO completely eliminates these issues and offers smoother and more continuous clock behavior. By employing the MBCO, the reconvergence period of coordinate parameters can be significantly reduced, leading to improved positioning accuracy.

For GPS broadcast ephemeris, the discontinuities are relatively small compared with those of BDS-3, typically at the centimeter level and occasionally reaching a few decimeters. The update period of the GPS broadcast ephemeris is 2 h; thus, the discontinuity frequency is also smaller than that of BDS-3. Overall, the GPS broadcast ephemeris has a smaller clock continuity than the BDS-3 broadcast ephemeris, and consequently, the positioning errors caused by this discontinuity are smaller. It is expected that the impact on the coordinate solution will not be as significant as that for BDS-3.

For Galileo, considering the frequent ephemeris updates at every 10 min, the clock discontinuities are minimal, to the extent that the difference between the original clock values and the MBCO is negligible. In Figure 6, the Galileo MBCO and the original clock are almost identical, with a difference of a few centimeters. In most cases, this difference can essentially be ignored. As a result, the Galileo MBCO will not have a substantial impact. Consequently, the impact of the MBCO on Galileo will not be discussed in subsequent analyses of positioning results.

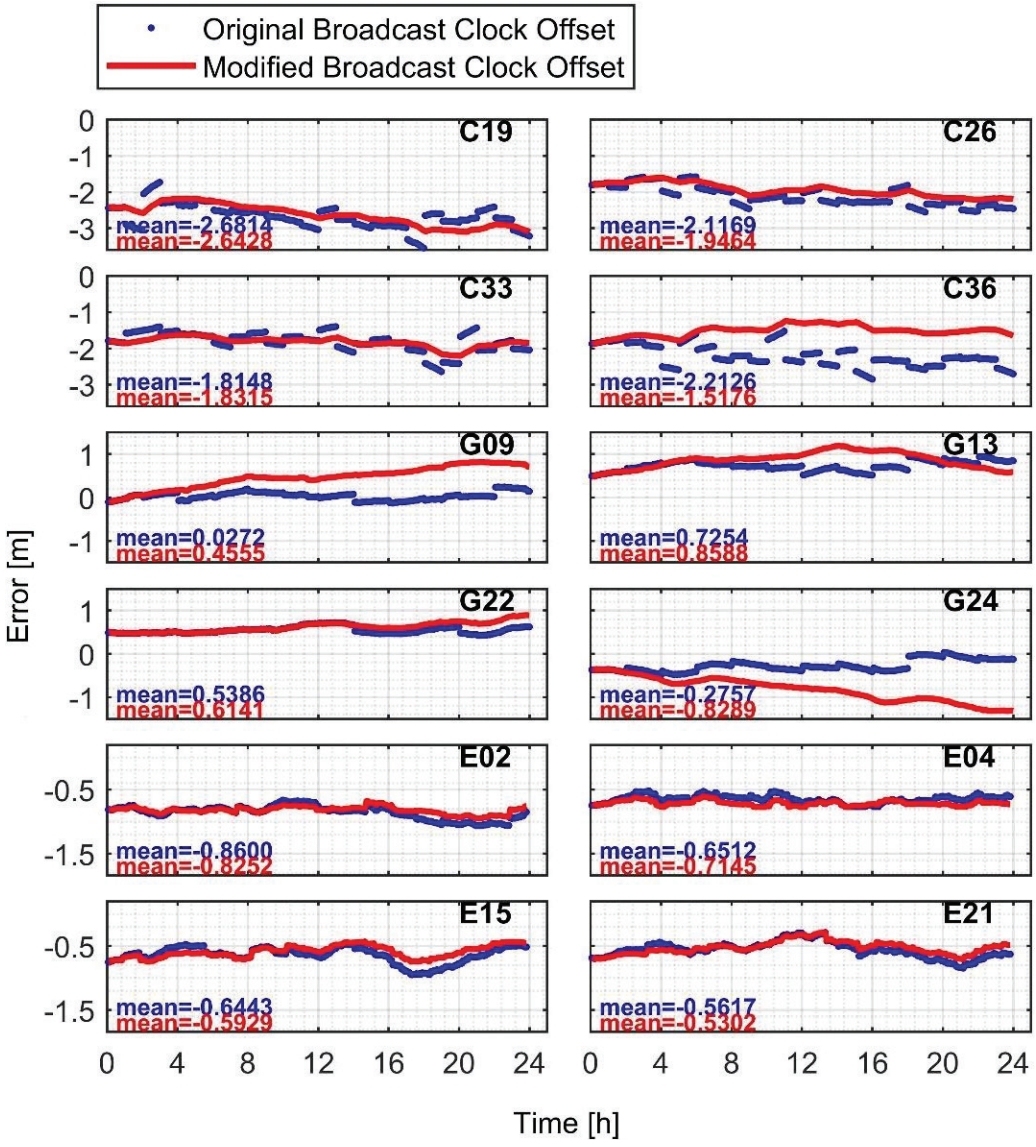

FIGURE 6 Comparison of the original clock offset and MBCO
Blue lines represent the original clock offset, whereas red lines represent the MBCO. Mean values are displayed at the bottom of each subplot.

4 | METHODS

In this study, four primary positioning modes, namely BRD_sto, BRD_est, mBRD_sto, and mBRD_est, are utilized. BRD_sto is the traditional BE-PPP mode, which uses the raw broadcast ephemeris for positioning and does not estimate SISRE parameters. BRD_est is a BE-PPP mode that still uses the raw broadcast ephemeris but incorporates an SISRE parameter estimation algorithm. This method has been proven effective in previous studies (Carlin et al., 2022; G. Chen et al., 2022). mBRD_sto is a new mode proposed in this study, enhancing BRD_sto with the MBCO. mBRD_est, another new mode, builds on BRD_est by applying the MBCO.

To investigate the influence of the MBCO in conventional BE-PPP, it is useful to compare BRD_sto and mBRD_sto. These two modes do not use the SISRE estimation described earlier and apply only the conventional BE-PPP method. Because different broadcast ephemerides are used, including the original broadcast ephemeris and the MBCO, the value in the stochastic model of the observations

should be reconsidered. Typically, the stochastic model is expressed as follows (Zhang et al., 2019):

$$\begin{aligned}\sigma_i^2 &= \sigma_{P_i}^2 + \sigma_{trop,i}^2 + \sigma_{iono,i}^2 + \sigma_{eph,i}^2 \\ \sigma_{eph,i}^2 &= \sigma_{orbit,i}^2 + \sigma_{clk,i}^2\end{aligned} \tag{3}$$

where i is the satellite number and $\sigma_{P_i}^2$ is the variance of pseudorange observations. $\sigma_{trop,i}^2$ and $\sigma_{iono,i}^2$ are the variance of troposphere and ionosphere model errors, respectively, and in the ionosphere-free combination, the latter is generally set to 0. $\sigma_{eph,i}^2$ is the sum of the squares of the troposphere and ionosphere model errors, and $\sigma_{orbit,i}^2$ and $\sigma_{clk,i}^2$ are the variance of orbit and clock errors introduced by the ephemeris. Typically, in PPP with precise ephemeris, the orbit and clock errors are assumed to be negligible, and thus, $\sigma_{orbit,i}^2$ and $\sigma_{clk,i}^2$ are commonly set to zero. In contrast, orbit and clock errors are not negligible in BE-PPP; thus, it is necessary to consider these errors in the stochastic model. To find the optimal σ_{eph}, we used one-dimensional sensitivity analysis, as shown in the left panel of Figure 7. For BRD_sto, when the process noise is set within the range of 0–15 cm, the positioning error gradually decreases, reaching an optimum at 15 cm and then leveling off. For mBRD_sto, the optimum occurs at 9 cm.

The BRD_est and mBRD_est modes applied in this study follow the methodology employed by Carlin et al. (2021) and G. Chen et al. (2022), except that the mBRD_est mode employs the MBCO. This method includes the projected orbit and clock errors as an additional parameter s in the pseudorange and carrier-phase observations. The observation equations are as follows:

$$p = \rho + \xi + c\left(\mathrm{d}t_r - \mathrm{d}t^s\right) + (T + \mathrm{d}T) + s + e \tag{4}$$

$$\varphi = \rho + \zeta + c\left(\mathrm{d}t_r - \mathrm{d}t^s\right) + (T + \mathrm{d}T) + s + \lambda(A + \omega) + \epsilon \tag{5}$$

where p and φ are the ionosphere-free combination of pseudorange and carrier-phase measurements, ρ is the geometrical range between the satellite's and the receiver's antenna reference points, c is the speed of light, $\mathrm{d}t_r$ and $\mathrm{d}t^s$ are

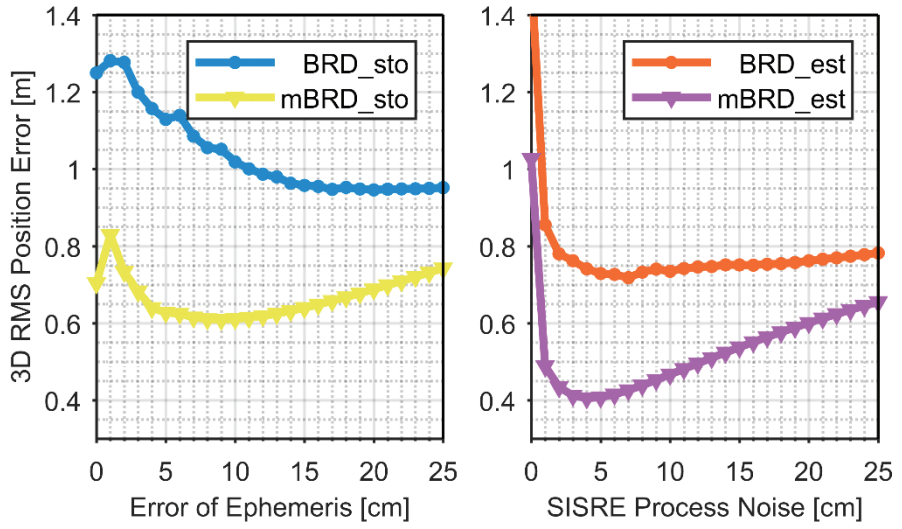

FIGURE 7 Position accuracy under different parameter settings for BDS-3

The figure on the left shows the variation in positioning accuracy for different σ_{eph} values, and the figure on the right shows the variation for different SISRE process noise values.

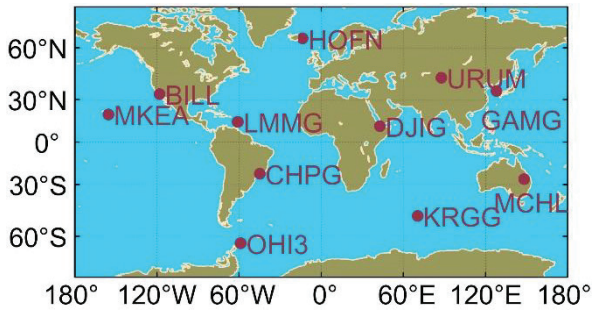

FIGURE 8 Map of the IGS stations used in this study

the receiver and satellite clock offsets, T is the modeled tropospheric delay, $\mathrm{d}T$ is an additional estimated tropospheric delay correction, λ is the wavelength of the ionosphere-free combination, A is the float-valued ionosphere-free combination of carrier-phase ambiguities, ω is the carrier-phase wind-up, and e and ϵ are the combined noise and multipath errors for the pseudorange and carrier phase. The state vector of the Kalman filter is now as follows:

$$\underline{x} = [x_r \quad y_r \quad z_r \quad \mathrm{d}t_r \quad \mathrm{d}T \quad s_0 \ldots s_n \quad A_0 \ldots A_n] \tag{6}$$

where $[x_r \quad y_r \quad z_r]$ is the receiver position vector and $s_0 \ldots s_n$ are the projected SISRE values for n tracked satellites.

To find the optimal process noise of the SISRE parameter, a one-dimensional sensitivity analysis was employed, as shown in the right panel of Figure 7. For BRD_est, when the process noise is set within the range of 0–7 cm, the positioning error decreases significantly, reaching an optimum at 7 cm, and then gradually increases. For mBRD_est, the optimum occurs at 4 cm. Figure 7 was derived from the positioning results of seven days from the 11 stations shown in Figure 8. All process noise settings were based on a time interval of 3600 s. It is worth noting that Figure 7 only shows the analysis for BDS-3. The results for GPS are similar and thus are not shown. We also conducted a similar analysis for the initial variance of SISRE parameters and found that their impact on positioning results is minimal. Typically, setting these parameters to match the SISRE of the corresponding broadcast ephemeris is suitable.

Table 1 provides the details of all positioning modes used in this research, with the first eight modes representing single-system modes and the remainder being multi-system modes. The first four modes use the BDS-3 system, whereas modes five to eight use the GPS system. All of the multi-system modes incorporate the SISRE estimation method. However, the variation among these modes is based on the selective use of the MBCO in certain systems. For example, mBRD_est(GC,G) indicates a mode using GPS and BDS-3 systems in which only GPS employs the MBCO. Similarly, mBRD_est(GCE,GC) indicates that all three systems are used, but only GPS and BDS-3 use the MBCO.

5 | PROCESSING STRATEGY

To evaluate the performance of the MBCO, we collected GPS (L1L2), Galileo (E1E5a), and BDS-3 (B1CB2a) observations from 11 IGS stations worldwide, as depicted in Figure 8. The statistics were based on a 7-day data set from June 1 to June 7, 2021. The specific details of each station are shown in Table 2. The specific configuration details of the PPP are presented in Table 3.

6 | KINEMATIC BE-PPP RESULTS

The kinematic positioning accuracy statistics of BDS-3 and GPS at 11 stations are shown in Figure 9 and Figure 10. The results are based on a week of observations and ephemeris data from June 1 to 7, 2021. The convergence time is 1 h, and the root mean square (RMS) of the positioning error, calculated from the second hour to the end of the day, is used to evaluate the positioning accuracy. More detailed statistics of our tests are presented in Table 4, Table 5, and Table 6.The statistics in Table 4 and Table 5 show the positioning accuracy of BDS-3 and GPS. The statistics in Table 6 show the multi-system positioning accuracy. The weekly final solution provided by the IGS is used as a reference in this study.

In Figure 9, the three-dimensional (3D) positioning accuracies of BRD_sto(C) and mBRD_sto(C) are approximately 1.0 m and 0.5 m, respectively. However, after the MBCO is applied, the positioning error of mBRD_sto (C) is reduced by almost half compared with BRD_sto (C), demonstrating that the MBCO can improve the positioning accuracy even without an estimation of the SISRE.

The two modes applying a SISRE estimation technique, BRD_est(C) and mBRD_est(C), exhibit similar behavior. The positioning accuracies of BRD_est(C) and mBRD_est(C) are approximately 0.7 m and 0.35 m, respectively. The positioning error of mBRD_est(C) is reduced to half of that of BRD_est(C) after the MBCO is applied. Before the MBCO is applied, the errors from broadcast ephemeris do not fully comply with the random walk assumption. However, with the implementation of the MBCO, these errors become consistent with this assumption, enhancing the effectiveness of the SISRE estimation method.

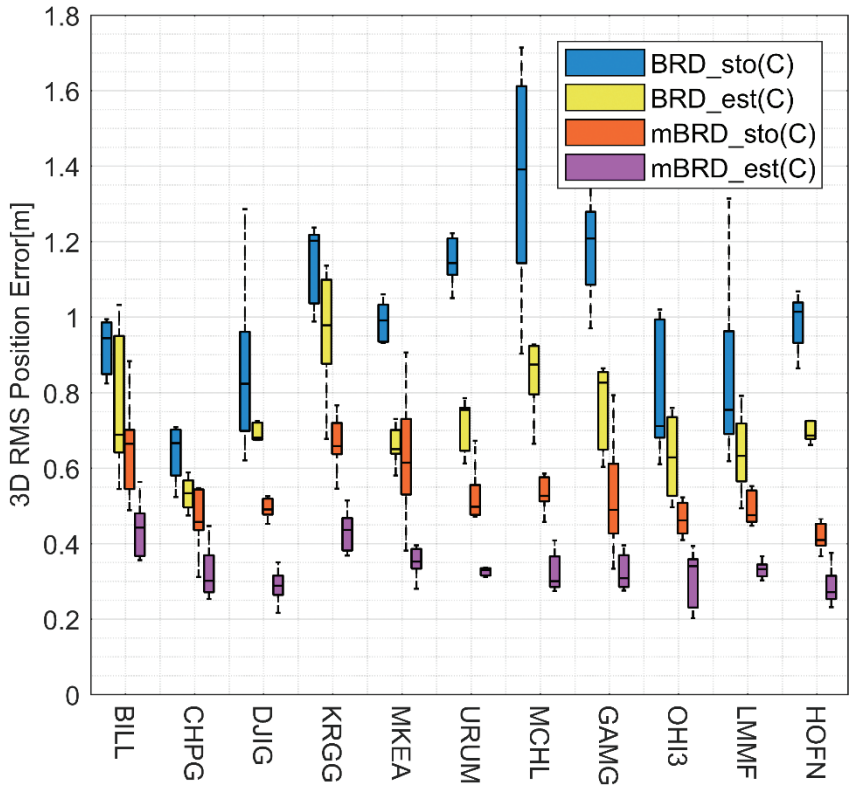

FIGURE 9 BE-PPP results (3D RMS) of BDS-3 for 11 IGS stations in kinematic mode
The three horizontal lines of the colored rectangles represent the first, second, and third quartiles of the distribution. The vertical lines extend to the maximum and minimum values. Outliers are not plotted.

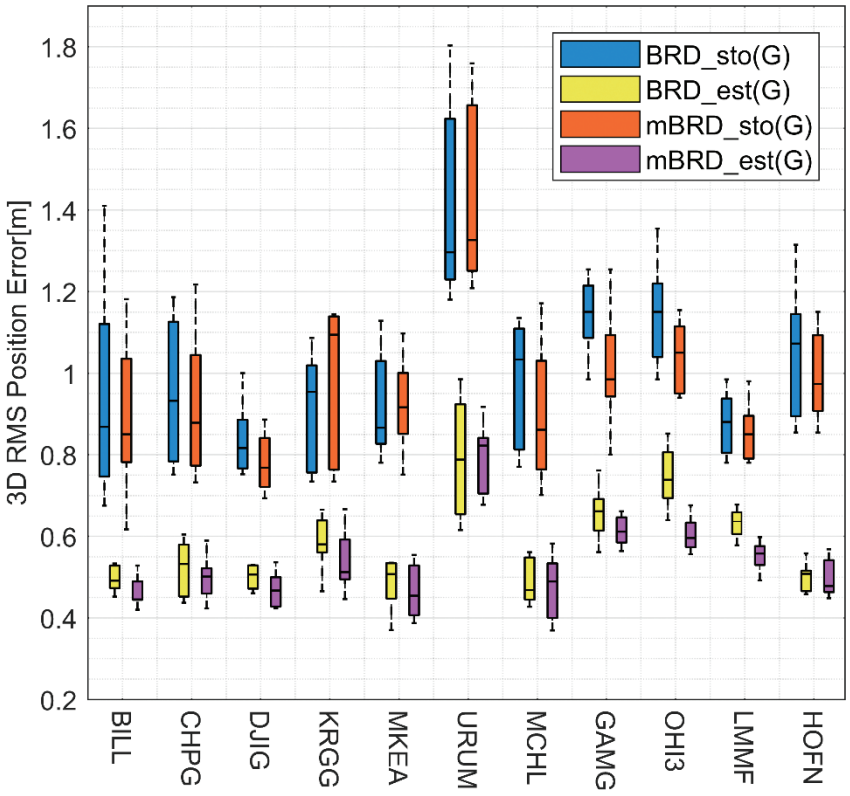

FIGURE 10 BE-PPP results (3D RMS) of GPS for 11 IGS stations in kinematic mode
The three horizontal lines of the colored rectangles represent the first, second, and third quartiles of the distribution. The vertical lines extend to the maximum and minimum values. Outliers are not plotted.

TABLE 4
BE-PPP Statistics in Kinematic Mode for BDS-3 from June 1 to 7, 2021 (Unit: cm)

	N	E	U	3D
BRD_sto(C)	33.52	38.91	83.55	99.36
BRD_est(C)	29.32	31.76	56.72	72.38
mBRD_sto(C)	17.23	25.16	43.06	53.61
mBRD_est(C)	12.89	17.43	25.32	33.96

TABLE 5
BE-PPP Statistics in Kinematic Mode for GPS from June 1 to 7, 2021 (Unit: cm)

	N	E	U	3D
BRD_sto(G)	31.45	38.69	85.14	98.67
BRD_est(G)	22.84	27.33	46.97	59.58
mBRD_sto(G)	30.13	37.55	82.96	93.70
mBRD_est(G)	20.38	26.75	42.75	53.18

For GPS, the positive effect of the MBCO is relatively small. Figure 12 shows that the accuracy of mBRD_sto(G) is slightly better than that of BRD_sto(G), displayed by blue and yellow bars. Moreover, the accuracy of mBRD_est(G) is slightly better than that of BRD_est(G), with an improvement of a few centimeters. Compared with BDS-3, the effect of the MBCO on GPS is much smaller. The GPS ephemeris

TABLE 6
BE-PPP Statistics in Kinematic Mode for Multi-System Solutions from June 1 to 7, 2021
For additional details about the modes in the table, please refer to Table 1 (unit: cm).

	N	E	U	3D
mBRD_est(GC,C)	15.30	12.32	24.82	31.65
mBRD_est(GC,G)	14.52	15.29	30.00	36.67
mBRD_est(GCE,C)	8.63	11.31	19.04	23.77
mBRD_est(GCE,G)	9.75	12.34	21.03	26.26
mBRD_est(GCE,GC)	8.62	8.15	18.72	22.16

updates more slowly, generally at an interval of 2 h, and the discontinuity is smaller (G. Chen et al., 2022), resulting in a smaller impact on the positioning accuracy.

More detailed statistical results are shown in Table 4 and Table 5, which correspond to the results in Figure 9 and Figure 10. The modes that apply the MBCO show better performance than the modes without the MBCO. In modes only including BDS-3 satellites, the improvement brought by the MBCO is substantial, corresponding to approximately 50% compared with the modes without the MBCO. For BRD_est(C), an accuracy of 72.4 cm is achieved, which is similar to the accuracy of 70.9 cm reported by G. Chen et al. (2022). mBRD_est(C) achieves an accuracy of 33.9 cm, which is very close to the accuracy of 31.7 cm reported by Carlin et al. (2021) for Galileo. These results confirm that use of the MBCO in BE-PPP can result in an accuracy improvement of nearly 40 cm for BDS-3 and can reach the high accuracy of Galileo.

For BRD_sto(G) and mBRD_sto(G), the MBCO contributes a 5-cm accuracy improvement, corresponding to approximately 5%. For BRD_est(G) and mBRD_est(G), the MBCO contributes a 6-cm accuracy improvement, corresponding to approximately 10%. Although the improvement achieved by the MBCO in these cases is not as substantial as that for BDS-3, these results demonstrate that the MBCO is effective in suppressing ephemeris jumps. Furthermore, for larger and more frequent jumps, the MBCO plays a more significant role.

The results in Table 4 show better performance than single-system solutions. For mBRD_est (GC,C) and mBRD_est (GCE,C), the results show an improvement of 8 cm and 3 cm compared with those without the MBCO, respectively. For mBRD_est (GC,G) and mBRD_est (GCE,G), the results show an improvement of 2 cm and 1 cm compared with those without the MBCO, respectively. Thus, the MBCO can still introduce an improvement of 5%–18% in multi-system solutions. For multi-system solutions, when the MBCO of the GPS and BDS-3 dual system was used in mBRD_est(GCE,GC) mode, the highest positioning accuracy of 22 cm was achieved, as shown in Table 6.

Figure 11 and Figure 12 show the average BE-PPP absolute error time series for BDS-3 and GPS from June 1 to 7, 2021. In Figure 11, a significant decline with respect to the magnitude of the position error is evident, and the continuity of the error time series is better, with almost no time-dependent error variation. In Figure 12, the error curves become smoother, and the discontinuity is also almost eliminated.

7 | STATIC BE-PPP RESULTS

The 3D RMSs of the 11 stations in static mode are depicted in Figure 13 and Figure 14. The static PPP takes the absolute value of the position error in the last epoch of the day as the RMS of the day. The accuracies of the various modes are

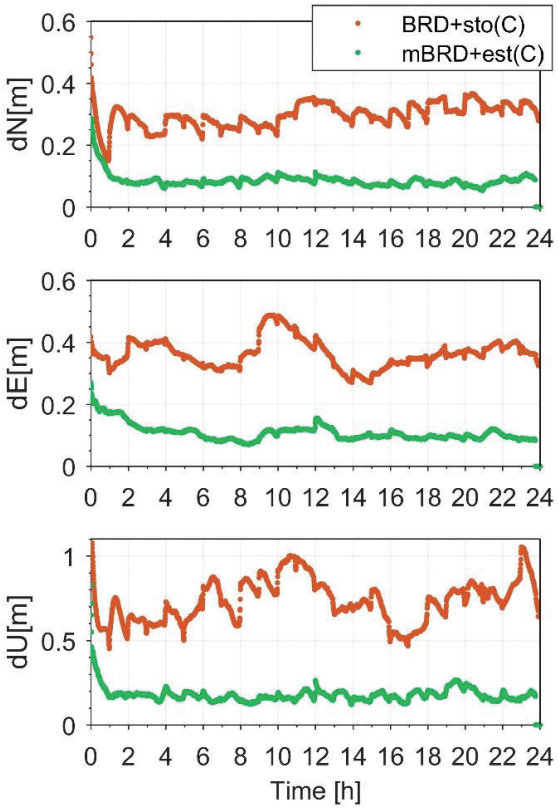

FIGURE 11 Average BE-PPP absolute error time series for BDS-3 from June 1 to 7, 2021 The position error series is based on the method with the MBCO.

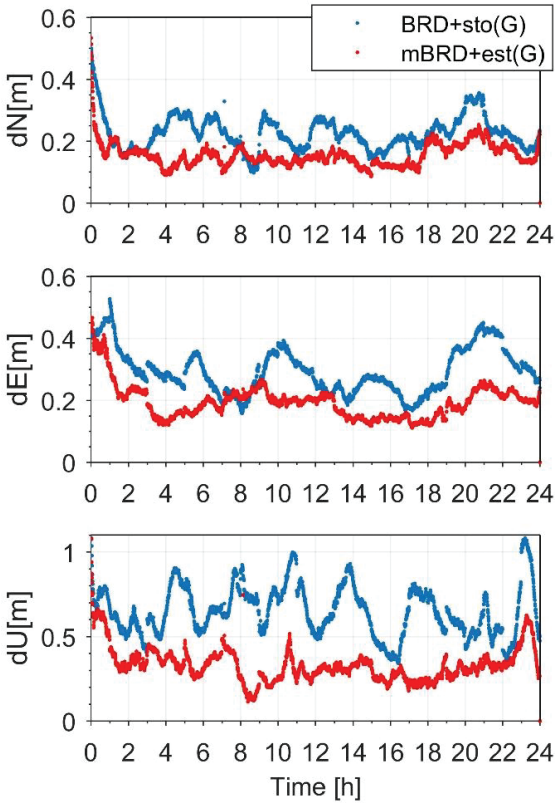

FIGURE 12 Average BE-PPP absolute error time series for GPS from June 1 to 7, 2021 The position error series is based on the method with the MBCO.

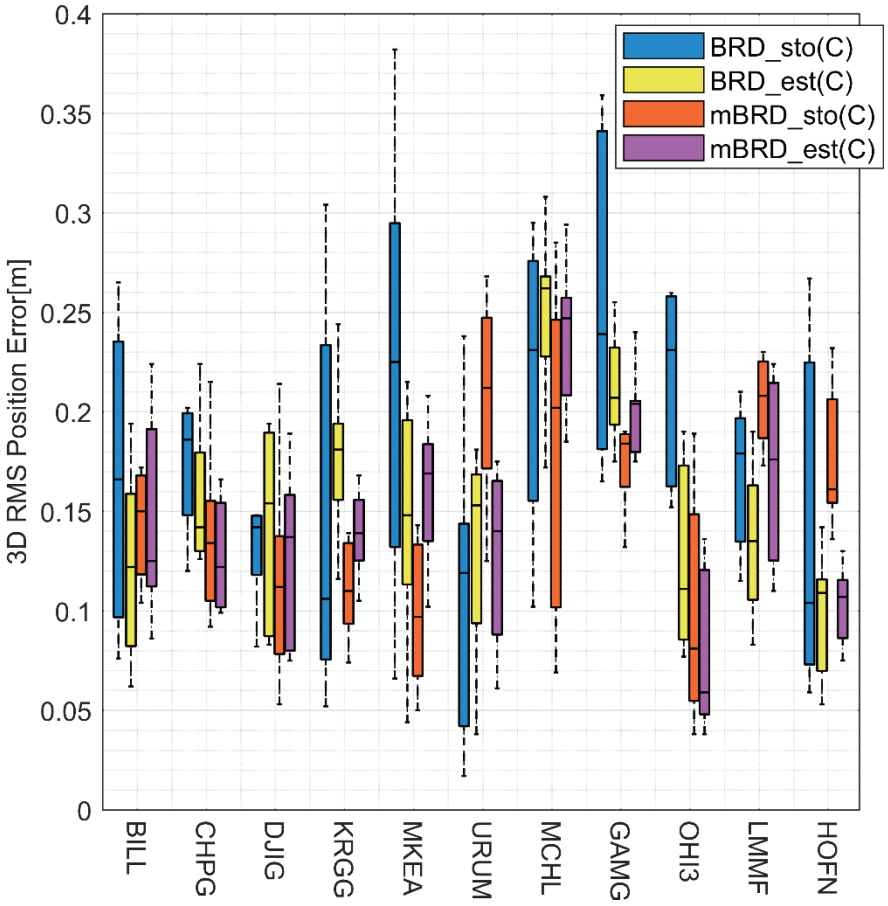

FIGURE 13 BE-PPP results (3D RMS) for 11 IGS stations in static mode from June 1 to 7, 2021

The three horizontal lines of the colored rectangles represent the first, second, and third quartiles of the distribution. The vertical lines extend to the maximum and minimum values. Outliers are not plotted.

basically distributed from 5 cm to 25 cm, and the differences between them are small. Comparing BRD_sto(C) and mBRD_sto(C), the 3D RMS decreases by 3 cm, with an improvement of 14.1%. Comparing BRD_est(C) and mBRD_est(C), the improvement is not significant at less than 1 cm, corresponding to an improvement of 5.3%. For mBRD_est(GC,C) and mBRD_est(GCE,C), the improvement is in millimeters. However, we can still deduce that the implementation of the MBCO has a positive impact on BE-PPP in static mode. Considering that the improvement in static mode is small, the 24-h solution time series is not demonstrated.

For kinematic modes, mBRD_est(C) consistently exhibits the highest positioning accuracy, as evidenced in Figure 9 and Tables 7–9. However, in static modes, mBRD_est(C) does not always perform optimally at some stations, as shown in Figure 13, even though it shows the best performance in Table 5. This result arises because static positioning accuracy is determined by the final epoch of the positioning period. Temporal impacts of ephemeris jumps are mitigated over time with data accumulation, leading to minor differences between modes. In contrast, kinematic positioning accuracy reflects the cumulative influence at every moment after convergence. Each accuracy degradation caused by ephemeris jumps impacts the overall accuracy, making the role of the MBCO more pronounced. Given this context, all static modes achieve high accuracy

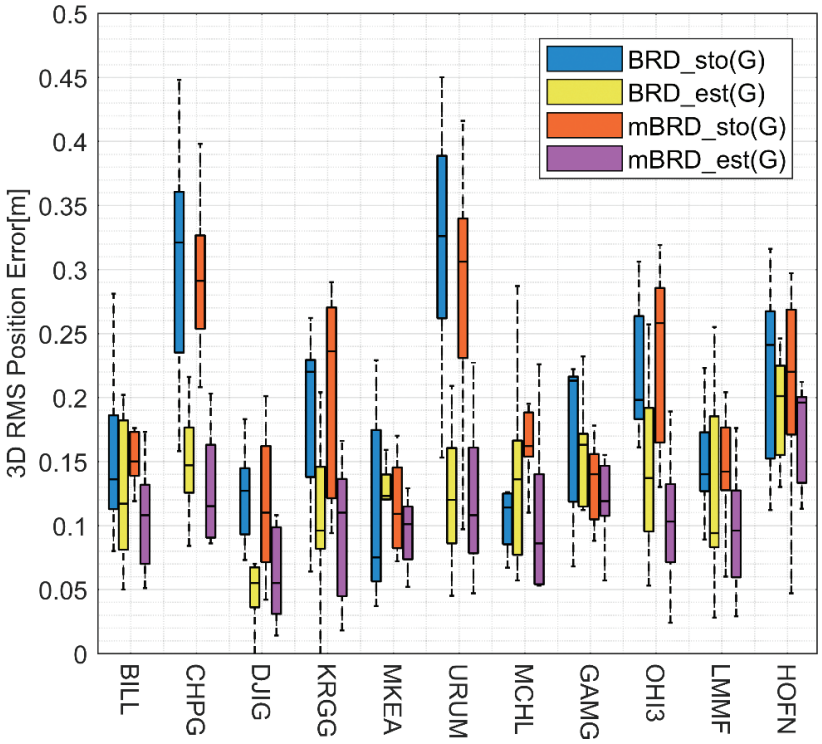

FIGURE 14 BE-PPP results (3D RMS) of GPS for 11 IGS stations in static mode from June 1 to 7, 2021
The three horizontal lines of the colored rectangles represent the first, second, and third quartiles of the distribution. The vertical lines extend to the maximum and minimum values. Outliers are not plotted.

TABLE 7
BE-PPP Statistics for BDS-3 in Static Mode from June 1 to 7, 2021

	N	E	U	3D
BRD_sto(C)	5.40	8.86	12.16	17.87
BRD_est(C)	4.41	8.70	9.41	15.41
mBRD_sto(C)	5.11	8.15	9.44	15.35
mBRD_est(C)	5.11	7.63	8.84	14.59

TABLE 8
BE-PPP Statistics for GPS in Static Mode from June 1 to 7, 2021

	N	E	U	3D
BRD_sto(G)	4.96	7.76	12.20	17.46
BRD_est(G)	8.00	8.78	9.22	16.93
mBRD_sto(G)	4.97	7.80	12.36	17.53
mBRD_est(G)	6.29	7.91	8.24	15.10

with minimal variation. Occasionally, the additional parameters estimated in mBRD_est(C) might increase inter-parameter correlations; thus, this mode may not always be optimal. However, as shown in Table 5, mBRD_est(C) remains the best mode, even though the accuracy improvement might be in the range of only a few centimeters.

TABLE 9
BE-PPP Statistics for a Multi-System in Static Mode from June 1 to 7, 2021
"(GC,G)" denotes the use of GPS and BDS-3 satellites, with the MBCO used only for GPS. For additional details about the modes in the table, please refer to Table 1 (unit: cm).

	N	E	U	3D
mBRD_est(GC,C)	5.43	4.47	6.26	10.67
mBRD_est(GCE,C)	3.91	3.14	4.87	8.02
mBRD_est(GC,G)	4.61	4.73	6.18	10.35
mBRD_est(GCE,G)	3.32	3.28	4.98	8.23
mBRD_est(GCE,GC)	2.95	3.07	4.89	7.92

8 | CONCLUSION

In this study, we addressed the issue of positioning error jumps in BE-PPP due to broadcast ephemeris discontinuities. We developed a solution by calculating the jump values between two sets of broadcast ephemerides in the orbit and clock and by compensating for them in subsequent clock values. This approach, based on the MBCO, effectively smooths out ephemeris jumps.

Using 7-day observational data from 11 IGS stations, our experiments demonstrated significant improvements in both kinematic and static modes. For the BDS-3 system, the kinematic positioning accuracy reached 34 cm, a reduction of over 50% compared with existing BE-PPP methods, and the static accuracy was 15 cm, corresponding to a 5%–10% improvement. For GPS, the kinematic accuracy improved to approximately 50 cm, i.e., a 10% increase, and the static accuracy improved to 15 cm, corresponding to an 8% improvement. Because ephemeris jumps are less frequent and less pronounced in GPS than in BDS-3, the improvements were less noticeable. In multi-system modes, the kinematic accuracy reached 22 cm, and the static accuracy was within 8 cm, showing the effectiveness of the MBCO in multi-system solutions.

Overall, the MBCO significantly enhances BE-PPP, promoting its further application. For autonomous orbit determination of low earth orbit satellites using broadcast ephemeris, the method proposed in this paper may mitigate the impact of ephemeris jumps, particularly for those utilizing BDS-3 observational data. The approach also has practical applications on the ground, such as in areas without internet or satellite-based correction data. Using broadcast ephemeris, our method can still provide decimeter-level kinematic positioning services, which is adequate for many situations. However, the proposed method does have limitations; for instance, it seems ineffective when the positioning duration falls entirely within a single IODE.

ACKNOWLEDGMENTS

We acknowledge the IGS for providing GNSS observation data and products. We thank the Helmholtz-Centre Potsdam - German Research Centre for Geosciences for providing precise orbit and clock products for comparison. This work was primarily funded by the Program of Shanghai Academic/Technology Research Leader (No. 20XD1404500), National Natural Science Foundation of China (No. 11673050, No. 41904034), and Opening Project of Shanghai Key Laboratory of Space Navigation and Positioning Techniques (No. 202114).

REFERENCES

Carlin, L., Hauschild, A., & Montenbruck, O. (2021). Precise point positioning with GPS and Galileo broadcast ephemerides. *GPS Solutions, 25*(2), 77. https://doi.org/10.1007/s10291-021-01111-4

Carlin, L., Montenbruck, O., Furthner, J., & Hauschild, A. (2022). UTC and GNSS system time access using PPP with broadcast ephemerides. *GPS Solutions, 26*(4), 142. https://doi.org/10.1007/s10291-022-01326-z

Chen, G., Wei, N., Li, M., Zhao, Q., & Zhang, J. (2022). BDS-3 and GPS/Galileo integrated PPP using broadcast ephemerides. *GPS Solutions, 26*(4), 129. https://doi.org/10.1007/s10291-022-01311-6

Chen, J., Li, H., Wu, B., Zhang, Y., Wang, J., & Hu, C. (2013). Performance of real-time precise point positioning. *Marine Geodesy, 36*(1), 98–108. https://doi.org/10.1080/01490419.2012.699503

Chen, J., Wang, J., Yu, C., Zhang, Y., & Wang, B. (2022). Improving BDS broadcast ephemeris accuracy using ground-satellite-link observations. *Satellite Navigation 3*, 11. https://doi.org/10.1186/s43020-022-00072-4

Chen, J., Zhang, Y., Yu, C., Wang, A., Song, Z., & Zhou, J. (2022). Models and performance of SBAS and PPP of BDS. *Satellite Navigation, 3*(1), 4. https://doi.org/10.1186/s43020-022-00065-3

CSNO. (2020). BeiDou Navigation satellite system signal in space interface control document service signal PPP-B2b (Version 1.0). China Satellite Navigation Office.

Elsobeiey, M., & Al-Harbi, S. (2016). Performance of real-time precise point positioning using IGS real-time service. *GPS Solutions, 20*(3), 565–571. https://doi.org/10.1007/s10291-015-0467-z

Geng, T., Jiang, R., Lv, Y., & Xie, X. (2022). Analysis of BDS-3 onboard clocks based on GFZ precise clock products. *Remote Sensing, 14*(6), 1389. https://doi.org/10.3390/rs14061389

Hadas, T., & Bosy, J. (2015). IGS RTS precise orbits and clocks verification and quality degradation over time. *GPS Solutions, 19*(1), 93–105. https://doi.org/10.1007/s10291-014-0369-5

Hadas, T., Kazmierski, K., & Sośnica, K. (2019). Performance of Galileo-only dual-frequency absolute positioning using the fully serviceable Galileo constellation. *GPS Solutions, 23*(4), 108. https://doi.org/10.1007/s10291-019-0900-9

Pan, L., Li, X., Yu, W., Dai, W., Kuang, C., Chen, J., Chen, F., & Xia, P. (2020) Performance evaluation of real-time precise point positioning with both BDS-3 and BDS-2 observations. *Sensors, 20*(21), 6027. https://doi.org/10.3390/s20216027

Malys, S., & Jensen, P. A. (1990). Geodetic point positioning with GPS carrier beat phase data from the CASA UNO experiment. *Geophysical Research Letters, 17*(5), 651–654. https://doi.org/10.1029/GL017i005p00651

Montenbruck, O., Steigenberger, P., & Hauschild, A. (2015). Broadcast versus precise ephemerides: A multi-GNSS perspective. *GPS Solutions, 19*(2), 321–333. https://doi.org/10.1007/s10291-014-0390-8

Yang, Y., Gao, W., Guo, S., Mao, Y., & Yang, Y. (2019). Introduction to BeiDou-3 navigation satellite system. *NAVIGATION, 66*(1), 7–18. https://doi.org/10.1002/navi.291

Yang, Y., Ding, Q., Gao, W., Li, J., Xu, Y., & Sun, B. (2022). Principle and performance of BDSBAS and PPP-B2b of BDS-3. *Satellite Navigation, 3*, 5. https://doi.org/10.1186/s43020-022-00066-2

Zhang, Y., Nobuaki, K., Chen, J., Wang, J., & Wang, H. (2019). Initial positioning assessment of BDS new satellites and new signals. *Remote Sensing, 11*(11), 1320. https://doi.org/10.3390/rs11111320

Zhang, Y., Chen, J., Feng-Yu, C., Ahao, W., & Jiexian, W. (2020). Apparent clock and TGD biases between BDS-2 and BDS-3. *GPS Solutions, 24*(1). https://doi.org/10.1007/s10291-019-0933-0

Zumberge, J., Heflin, M., Jefferson, D., Watkins, M., & Webb, F. H. (1997). Precise point positioning for the efficient and robust analysis of GPS data from large networks. *Journal of Geophysical Research: Solid Earth, 102*(B3), 5005–5017. https://doi.org/10.1029/96JB03860

How to cite this article: Cheng, Q., Chen, J., Zhang, Y., & Yu, C. (2024). Real-Time precise point positioning method considering broadcast ephemeris discontinuities. *NAVIGATION, 71*(2). https://doi.org/10.33012/navi.643